Three-Port Current Fed Push/Pull Partial Power Converter for Integration of PV/Battery Systems in DC Microgrids

Neelesh Yadav
Department of Electrical Power Engineering and Mechatronics
Tallinn University of Technology
Tallinn, Estonia
neelesh.yadav@taltech.ee

Andrii Chub
Department of Electrical Power Engineering and Mechatronics
Tallinn University of Technology
Tallinn, Estonia
andrii.chub@taltech.ee

Lauri Kütt
Department of Electrical Power Engineering and Mechatronics
Tallinn University of Technology
Tallinn, Estonia
lauri.kutt@taltech.ee

***Abstract*—The concept of a partial power converter (PPC) has been widely adopted to replace the full power converter. PPC processes only a fraction of the total power flowing between input and output, or source and load, which results in a very high efficiency and power density. Even though PPC has been used in two-port applications, further research is still required to understand PPC in multi-port applications fully. Thus, the main goal of this paper is to investigate a three-port PPC for integrating photovoltaic (PV)/battery systems in dc microgrids. This work proposes a dual-input single-output (DISO) system that forms the two PPC submodules by connecting a PV and a battery to the dc bus via an individual series port of dc-dc cell. Furthermore, this work provided a cost-effective soft switching solution using a current-fed resonant push-pull configuration in PPC. The suggested PV/battery system based on DISO-PPC architecture is validated using PSIM simulation in conjunction with PV and battery voltage variation, maximum power point tracking, and battery current management.**

***keywords*—Battery, dc-dc converter, partial power converter, PV, resonant push-pull converter, multi-port system.**

I. Introduction

THE partial power converters (PPCs) are an emerging technology that offers an approach to delivering significant amounts of power directly to the load while processing a small amount of total power owing to variations in voltage [1]-[5]. Compared to full power converters (FPCs), PPCs have several benefits, including high power density and efficiency, while they suffer from limited application flexibility [6]. Galvanically isolated dc-dc converter topologies, which have made significant advancements recently, provide the basis of the majority of PPC architectures [7]-[11]. Furthermore, the cost of a PPC is reduced as it processes a small percentage of the total power, which lessens the current and voltage stress on components [12]. PPCs demonstrated promising results in numerous applications, such as photovoltaic (PV) systems, electric vehicle charging, battery energy storage, and fuel cells [13].

PPCs can be categorized as step-up (SU), step-down (SD), or step-up/down (SU/D) converters, depending on how a particular PPC operates [3], [14], [15]. Depending on the input and output or source and load connections, a PPC can be classified as series-input parallel-output (SIPO) or parallel-input series-output (PISO). A SIPO configuration works better in voltage SD applications, whereas PISO works well in voltage SU applications [16]. State-of-the-art PPCs were mainly proposed for two-port applications. There is currently a research gap in expanding the PPC technology to multi-port applications. However, the multi-port PPC architecture has been presented in several articles. In addition to two-port applications, two three-port PPCs have been proposed in [17], [18]. In [17], a three-port SU PPC with fewer components was used to transfer power from the battery and PV modules to the output load. Authors of [18] proposed a decreased-rated multi-input converter for connecting hybrid energy storage systems to loads in automotive and microgrid applications.

The few existing multi-port PPCs are not easily scalable to different applications. In particular, an efficiency-optimized PPC design must utilize a high-gain galvanically isolated dc-dc cell to minimize voltage stress in the series port. A variety of isolated dc-dc converter topologies have been used in two-port PPCs, such as dual active bridge converters, phase-shifted full-bridge converters, and push-pull converters [4], [12], [19], [20]. Nevertheless, none of the existing three-port PPCs can be easily adopted in different applications. Hence, this paper proposes a new multi-port PPC suitable for high-power multi-port applications, such as dc microgrids, due to optimized isolated dc-dc cell use.

Two types of multi-port PPC structures are available in the literature: single-input multi-output (SIMO) and multi-input single-output (MISO). A MISO PPC system based on the active bridge concept was presented in [21]. One port of each module is connected to the others in this way to create a radial structure, and the input/output port is attached to a different terminal that is connected both in series and parallel. In order to incorporate energy storage for EV charging, a different three-port PPC generated from a triple active bridge is suggested in [22]. However, in this topology, a normal full-bridge full power converter is connected to another port, and just one full-bridge port operates as a series port of a PPC. In order to reduce this research gap in the multi-port PPCs, this paper proposes a scalable three-port PPC topology. Its main contributions can be summed up as follows:

- This work presented a dual-input and single-output (DISO) PPC topology for the integration of PV/battery (BAT) systems into dc microgrids.
- The proposed DISO PPC utilizes a soft-switching current-fed push-pull topology, which reduces the number of switches and, consequently, the implementation cost.

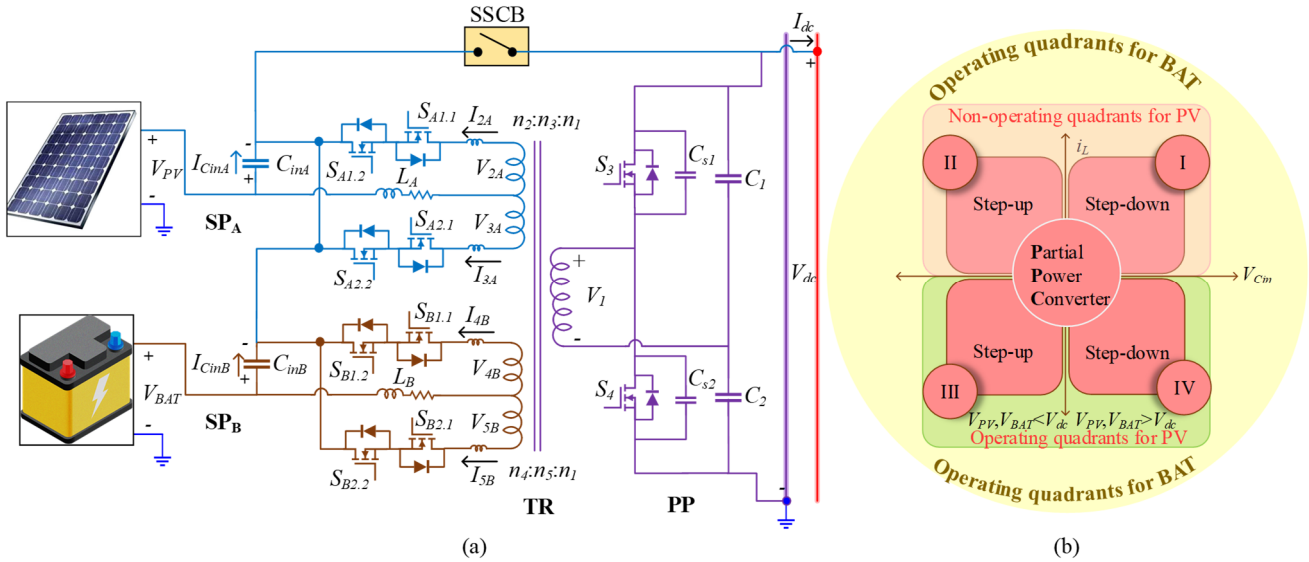

Fig. 1. DISO-PPC architecture proposed for integration of PV/battery systems (a) and its operating quadrants (b).

- A short resonant state is introduced into the modulation of the current-fed push-pull ports to enable complete soft-switching and, consequently, reduce switching losses.
- A control system is proposed to decouple the maximum power point tracking (MPPT) of a PV string from the battery current control.

II. Proposed Dual-Input Single-Output PPC Based on Current-Fed Push-Pull DC-DC Topology

Fig. 1(a) depicts the proposed DISO dc-dc current-fed push-pull PPC design. In this, the series ports of the PPC are formed by two PPC submodules made of dc-dc cells. SP_A and SP_B are the designators of these modules. Due to the consideration of a current-fed push-pull (CFPP) design, both SPs are connected to a five-winding high-frequency transformer (TR) and contain four switches each (SP_A: $SP_{A1.2}$, $SP_{A1.1}$, $SP_{A2.2}$, $SP_{A2.2}$ and SP_B: $SP_{B1.2}$, $SP_{B1.1}$, $SP_{B2.2}$, $SP_{B2.2}$). A half-bridge (switches: S_3, S_4 and capacitors: C_1, C_2) is connected at the primary winding of the TR, creating a parallel port on the PPC. In this case, it is essential to note that both series submodules, SP_A and SP_B, share a mutual parallel port. In this paper, a PV source is connected at SP_A and a BAT pack is attached to the SP_B of DISO CFPP-PPC. The voltage of PV and BAT are named V_{PV} and V_{BAT}, respectively, which are maintained between 320 and 380 V. Conversely, a dc bus (V_{dc}) connected to a parallel port is regulated at 350 V. Additionally, a solid-state circuit breaker (SSCB) is used in the direct line to provide fast protection in the event of a fault on either side.

Since a PPC can operate in both step-up (SU) and step-down (SD), these operating modes are decided based on the polarity of the voltage across the series capacitors (C_{in}: C_{inA}, C_{inB}), defined as V_{CA}, V_{CB}. Moreover, a PPC can also operate in all four quadrants, as shown in Fig. 1(b). It is worth mentioning that SP_A would always function in only two quadrants (Q_{III} and Q_{IV}) because of the unidirectional power flow from PV. Meanwhile, SP_B functions in all four quadrants as the BAT pack experiences bidirectional current. These operating quadrants are chosen by I_L and V_C (Fig. 1(b)). The PPC differential voltage range ($\Delta V_{CA}=V_{CA}= V_{PV} - V_{dc}$) and ($\Delta V_{CB}= V_{CB}= V_{BAT} - V_{dc}$) determines the maximum processed active power in the PPC ports SP_A and SP_B, respectively. The partiality factors and PPC gains are defined as K_{prA}, K_{prB} and G_A, G_B in Eqs. (1) and (2), respectively.

$$G_A = \frac{V_{dc}}{V_{PV}}; G_B = \frac{V_{dc}}{V_{BAT}} \tag{1}$$

$$K_{prA} = 1 - G_A; K_{prB} = 1 - G_B \tag{2}$$

III. Operation Principle of CFPP-PPC with Control Method Employing Decoupled Controllers

Fig. 2(a) shows the control structure for the BAT pack and PV string. Here, a typical proportional-integral (PI) controller is used to regulate the battery current. In this case, a reference current for the BAT controller is defined by $i_{BAT,ref}$. A mathematical expression of the PI controller is stated in (3) where $G_C(s)$ represents the controller gain.

$$G_C(s) = K_p + K_i \cdot \frac{1}{s} \tag{3}$$

This PI reduces zero steady-state error by providing an infinity dc gain. The integral and proportional gains are defined by K_i and K_p, respectively. The other controller performs MPPT to harvest the maximum power from the PV string. Several algorithms are available for this operation, but in this paper, a perturbation and observation (P&O) MPPT algorithm is used. The flow chart of this P&O MPPT algorithm is illustrated in Fig. 2(b). The control signals t_{revA} and t_{revB} produced by these controllers are later utilized to produce modulated pulses for the corresponding switches in series ports. A quadrant selector is utilized to choose the proper quadrant depending on the status of the voltages V_{CA}, V_{CB}, and currents i_{LA}, i_{LB}, because these modulated signals differ for each quadrant.

Fig. 3 exhibits the suggested modulation sequences and important current-voltage waveforms of CFPP-PPC for forward operation. There are some differences between this modulation and traditional modulation [23]. The proposed

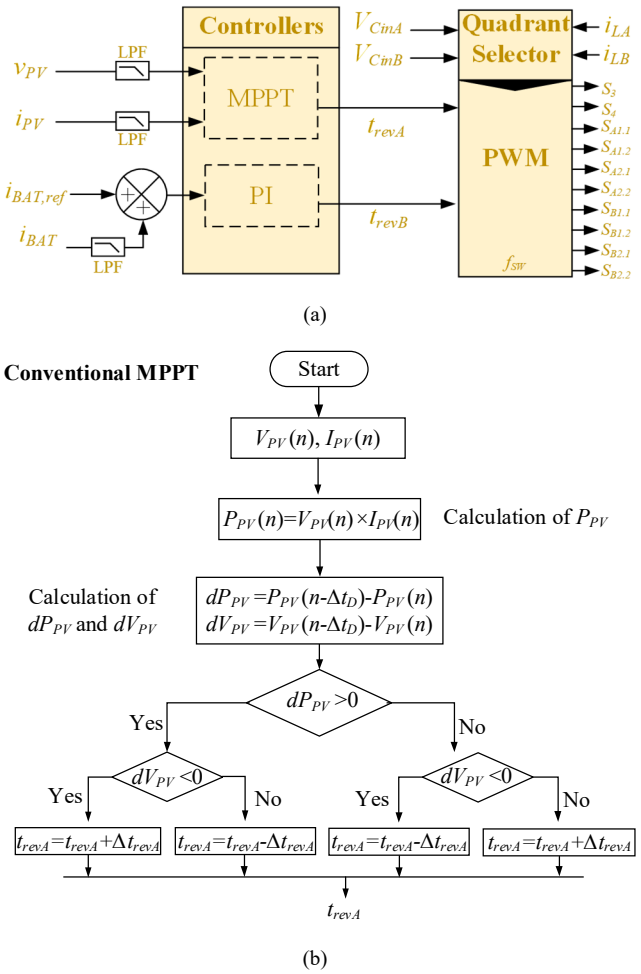

Fig. 2. Control of (a) PV/BAT system using the (b) MPPT algorithm.

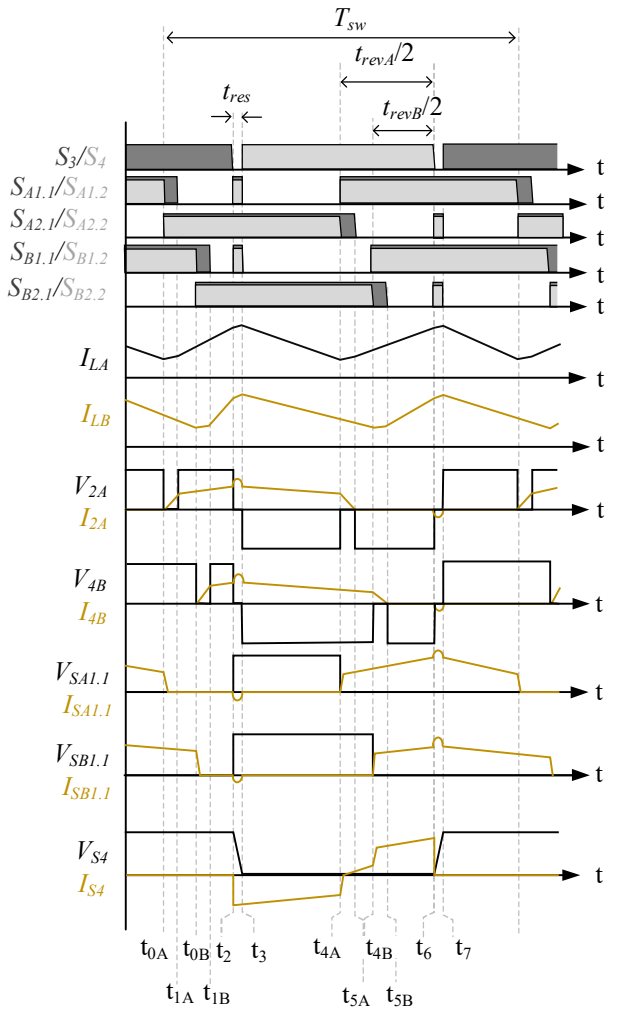

Fig. 3. Resonant push-pull modulation for CFPP-PPC converter for forward operation.

modulation reduces the charge-discharge durations of the PP side snubber capacitors (C_{s1}, C_{s2}) by including a resonant state. Even in the absence of operating power, the resonance mechanism generates enough energy to complete the charging and discharging of capacitors. Complete zero voltage switching (ZVS) is provided during this interval, leading to a notable decrease in switching power loss. Several operating intervals (t_0-t_7) (T_{sw}) are explained in Table I for half the switching period. The generalized voltage gain equation of push-pull PPC can be written as (4) [18].

$$G_{dc}(s) = \frac{V_{dc}}{V_C} = \frac{1}{1-2t_{rev}} \tag{4}$$

IV. Simulation Verification and Discussion

The digital PSIM simulation platform is used to verify the proposed PV-BAT-based multi-port DISO-CFPP-PPC. Table II provides the parameters and specifications of the simulated converter. Fig. 4 illustrates the SP switch voltages $V_{SA1.1}$, $V_{SA2.1}$ and currents $i_{SA1.1}$, $i_{SA2.1}$, and PP voltage V_{S3} and current i_{S3}. A correlation between the modulation concept and simulation result can be observed in Fig. 3 and Fig. 4.

To illustrate the dynamic operation of CFPP-PPC quadrants, the BAT and PV voltage are changed gradually. Three case studies have been tested where the DC bus voltage (V_{dc}) was kept constant at 350 V throughout the operation. In the first study, as shown in Fig. 5, the V_{BAT} is maintained at 320 V and feeds the power to the dc bus at the current of 5 A. Here, PPC port SP_B always operates in SU mode. In the beginning (instant t_0), the V_{PV} is around 325 V and MPPT tracks the maximum power of 1.480 kW in the SU mode (PPC port SP_A). Later, at the instant t_1, the PV string voltage V_{PV} starts to increase. As a result, the power harvested from the PV string, P_{PV}, also increases gradually. After a while, at the instant t_2, the PV string operating voltage approaches the value of V_{dc}. The PPC enters conditions that could be referred to as the dead zone [4].

The push-pull modulation allows the PPC to operate in this dead zone and make the mode transition smoothly. This remarkable feature is associated with the operating principle of the CFPP, where circulating energy results in a sizable current ripple in the CFPP inductor, providing enough energy to achieve controllability at zero series port voltage. On the other hand, the circulating energy causes conduction losses in the isolation transformer and semiconductor components. As a result, the PPC mode transitions smoothly from SU to SD when the PV string voltage V_{PV} becomes greater than V_{dc}. At the instant t_3, the V_{PV} reaches the value of 365 V and settles in that operating point while delivering power of 1.60 kW to the dc bus. For this reason, CFPP is a superior solution where SU/D voltage regulation is required in a PPC.

TABLE I. PPC OPERATION STATES

State	Interval	Operation
State-I	t_{0A}-t_{1A}	The PP switch S_3 is turned off at the instant t_{0A}. Inductor L_A gains energy, and the converter enters a shoot-through state on the SP_A side. The body diode (BD) of switch $S_{A1.2}$ conducts the current i_{LA} when switch $S_{A1.2}$ is turned off. Simultaneously, the secondary side leakage inductance of the TR assists ZVS turn-on of the switch $S_{A2.1}$. A redistribution state is created when i_{LA} redistributes between $S_{A1.1}$ to $S_{A2.1}$. The cancellation of both winding fluxes causes the winding voltage V_{2A} to drop to zero. Later, at the instant t_{0A}, the current of the switch $S_{A1.1}$ drops to zero, so it can be turned off with ZCS. The energy transferred in the reverse direction from the PP side to the SP side during this interval ($t_{0A}<t<t_{1A}$) causes the converter to increase the dc voltage gain. Conversely, $S_{B2.1}$ and $S_{B2.2}$ are turned off while $S_{B1.1}$ and $S_{B1.2}$ are conducting current on the SP_B side.
State-II	t_{0B}-t_{1B}	At the instant t_{0B}, at the SP_A side, the power is transferred in the same manner as in State-I. In contrast, the converter goes into a shoot-through state on the SP_B side. The inductor L_B starts to increase stored energy in this state. When switch $S_{B1.2}$ is turned off, the current i_{LB} is conducted by the BD of $S_{B1.2}$. In addition, the secondary leaking inductance assists the ZVS turn-on of the switch $S_{B2.1}$. The current i_{LB} redistributes from $S_{B1.1}$ to $S_{B2.1}$. The secondary winding voltage V_{4B} drops to zero. After the instant t_{0B}, the current of the switch $S_{B1.1}$ is zero, so it can be turned off with ZCS.
State-III	t_2-t_3	At the instant t_2, the PP switch S_4 gets turned on with soft switching. By turning off both PP switches and turning on all SP_A and SP_B side switches, the resonant interval (t_{res}) can be created. Snubber capacitors and input inductance work together to form the resonant tank. The resonant state added to the modulation guarantees ZVS of the PP side switches.
State-IV	t_3-t_{4A}	At the instant t_3, switch S_4 gets turned on with ZVS, and power delivery (started in State-III) is maintained.
State-V	t_{4A}-t_{5A}	At the instant t_{4A}, on the SP_A side, the switch $S_{A2.2}$ is turned off, so its BD starts conducting. The switches $S_{A1.1}$ and $S_{A1.2}$ are turned on with ZCS supported by the leakage inductance of the TR. Next, the current i_{LA} is redistributed again from $S_{A2.1}$ to $S_{A2.2}$. On the SP_B side, the power flows in the same way as in the State-IV.
State-VI	t_{5A}-t_{4B}	During this interval, on the SP_A side, the switches $S_{A2.1}$ and $S_{A2.2}$ are turned off, whereas $S_{A1.1}$ and $S_{A1.2}$ are turned on and conduct current. On the SP_B side, the switch pairs $SB_{1.1}$, $SB_{1.2}$ and $SB_{2.1}$, $SB_{2.2}$ are turned off and turned on, respectively.
State-VII	t_{4B}-t_{5B}	At the instant t_{4B}, on the SP_A side, the power is transferred similarly to the State-V. On the other hand, on the SPB side, the switch $S_{B2.2}$ gets turned off, so BD starts to conduct the operation. Likewise, $SB_{1.1}$ and $SB_{1.2}$ get turned on with ZCS. This is another redistribution state for the SP_B module. The current i_{LB} gets redistributed from $SB_{2.1}$ to $SB_{1.1}$.
State-VIII	t_{5B}-t_6	This time interval is similar to State-VI for the SP_A side. On the SP_B side, the switch pairs $SB_{1.1}$, $SB_{1.2}$ and $SB_{2.1}$, $SB_{2.2}$ are completely turned on and off, respectively.

TABLE II SYSTEM SPECIFICATIONS

Parameter	Symbol	Value
Dc bus voltage	V_{dc}	350 V
Filter inductor	L_A, L_B	100 µH
Transformer TR_1 side leakage inductance and ESR	L_{eqP}, R_{eqP}	2µH 82 mΩ
Transformer TR_2 and TR_3 side leakage inductance and ESR	L_{eq2}, L_{eq3} R_{eq2}, R_{eq3}	0.6 µH 50 mΩ
Transformer TR_4 and TR_5 side leakage inductance and ESR	L_{eq4}, L_{eq5} R_{eq4}, R_{eq5}	0.6 µH 50 mΩ
Magnetizing inductance	L_{mA}, L_{mB}	2.5 mH
Transformer ratios	$n_2 : n_3 : n_1$	1:1:2
	$n_4 : n_5 : n_1$	1:1:2
Half-bridge capacitors	C_1 and C_2	66 µF
Snubber capacitors	C_{s1} and C_{s2}	1.1 nF
Series Capacitor	C_{inA}, C_{inB}	100 µF
Battery Voltages	V_{BAT}	320 V to 380 V
PV Voltage	V_{PV}	325 V to 365 V
Switching frequency	f_s	50 kHz
A step change in the MPPT control variable	Δt_{revA}	0.05 s
Time step	Δt_D	0.001 s

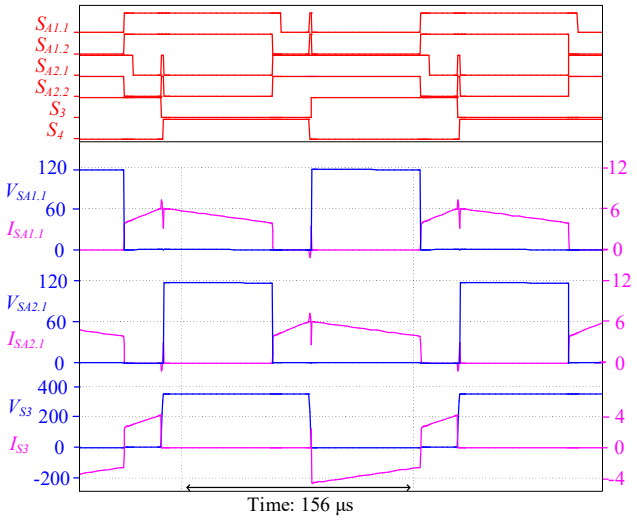

Fig. 4. Series and parallel side switch voltage and current waveform.

Another tested case study is shown in Fig. 6. In this scenario, the PV string voltage V_{PV} is stabilized at 365 V, so PPC port SP_A operates in SD mode to deliver a maximum PV string power of 1.60 kW. The SU operation of the PPC port

SP_B starts from t_0 with V_{BAT} = 320 V and I_{BAT} = 5 A. Next, at the instant t_1, the BAT pack voltage begins to rise, and after some time, at the instant t_2, it reaches close to V_{dc} (dead zone). As discussed above, PPC smoothly changes its quadrants and mode from SU to SD. It is worth mentioning here that the closed-loop control system uses a PI controller to calculate the phase shift for each mode based on the measured (i_{BAT}) and reference ($i_{BAT,ref}$) currents. A feed-forward control strategy is implemented throughout the mode change to minimize mode transition transients. This entails calculating the initial phase shift for the subsequent mode using the measured relevant data [15]. Later, at the instant t_3, the BAT pack voltage becomes constant at 380 V and feeds the dc bus. Therefore, the results assure the dynamic performance of a multi-port PPC for PV/BAT application.

In order to emulate a challenging scenario, the proposed multi-port PPC has been tested under dynamic conditions where the operating voltage of both PV and BAT is changing, as shown in Fig. 7. In this, at the beginning of the test, instant t_0, the PV string and BAT pack voltages equal 325 V and 320 V, respectively. Therefore, PPC series ports SP_A and SP_B operate in the SU mode, quadrant Q_{III}. At the instant t_1, both the voltages start to rise gradually. After a while, at the instant t_2, the BAT pack voltage V_{BAT} exceeded V_{dc}, and the controller smoothly changed the operating quadrant of the PPC port SP_A to Q_{IV}, so it starts working in the SD mode. Meanwhile, the PV string voltage V_{PV} reaches V_{dc} at the instant t_3 when PPC port SP_B shifts its quadrant to Q_{IV} (SD mode). After some

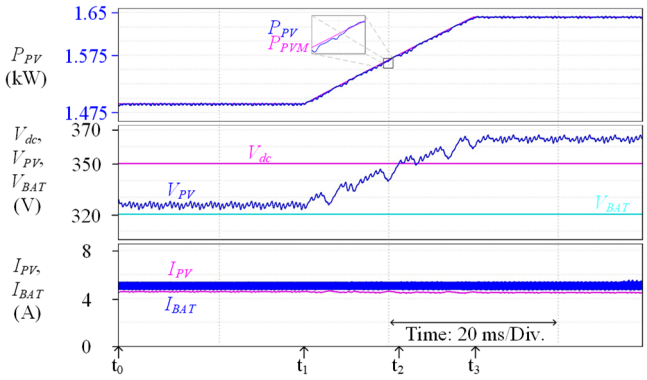

Fig. 5. PPC performance for varying V_{PV} (325 to 365V) while keeping constant V_{BAT} = 320 V and V_{dc} = 350 V.

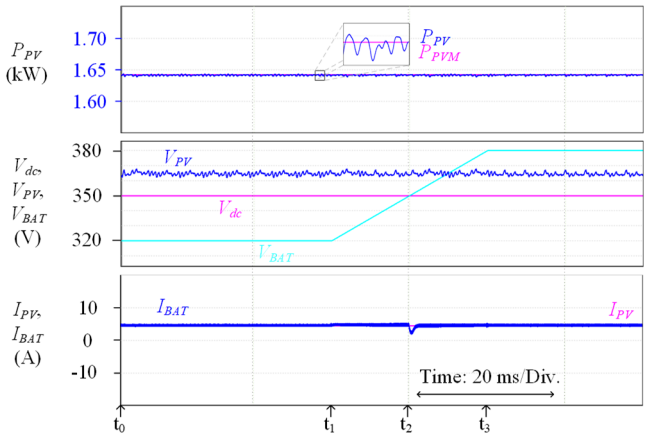

Fig. 6. PPC performance for varying V_{BAT} (320 to 380 V) while keeping constant V_{PV} = 365 V and V_{dc} = 350 V.

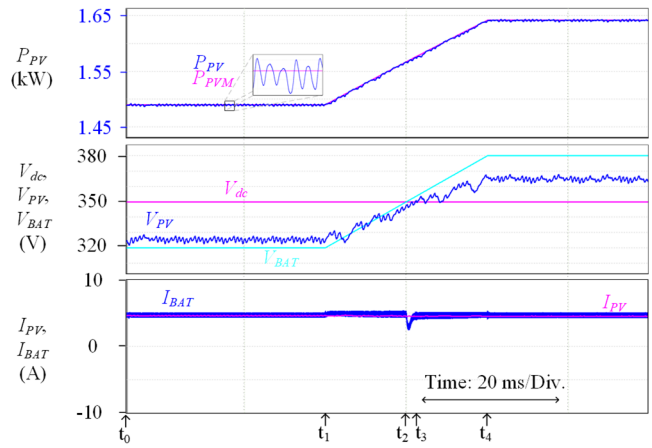

Fig. 7. PPC performance for varying V_{BAT} (320 to 380 V) and V_{PV} (325 to 365V) and constant V_{dc} = 350 V.

time, at the instant t_4, both voltages V_{PV} and V_{BAT} get settled at 365 V and 380 V, respectively, and operate in steady-state conditions.

V. Conclusions

This work proposes a resonant push-pull-based dual-input single-output PPC that integrates a PV and a battery pack operating at 320 V to 380 V with the 350 V dc bus. A five-winding transformer is required to implement this DISO CFPP-PPC, where PV and battery are linked to the series CFPP ports of the PPC. Furthermore, autonomous controls of battery current and maximum power point tracking are also achieved. The proposed architecture is evaluated for about 8% partiality and validated with PSIM simulation. The simulation result demonstrates the capability and sufficient performance of the DISO CFPP-PPC. The results have confirmed a good dynamic performance of PPC at 1.65 kW of power, irrespective of changes in PV and battery voltage. Moreover, a smooth transition of modes and quadrants is also observed using a novel CFPP modulation. This modulation features a resonant interval that ensures zero voltage switching of the semiconductor devices in the parallel PPC port. At the same time, the leakage inductances of the isolation transformer assist in zero current switching of the semiconductors in series ports.

Acknowledgments

This research was supported in part by the Estonian Research Council under the project RVTT3 "CERN Science Consortium of Estonia" and grant PRG2055, in part by the Estonian Centre of Excellence in Foundations of the Universe (grant TK202) funded by the Estonian Ministry of Education and Research, and in part by the European Union's Horizon Europe research and innovation programme under grant agreement no. 101136131. Views and opinions expressed in this document are those of the authors only and do not necessarily reflect those of the European Union or the European Climate, Infrastructure and Environment Executive Agency (CINEA). Neither the European Union nor the granting authority can be held responsible for them.

References

[1] N. Hassanpour, A. Blinov, A. Chub, D. Vinnikov and O. Abdel-Rahim, "A Series Partial Power Converter Based on Dual Active Bridge

Converter for Residential Battery Energy Storage System," 2021 IEEE 62nd International Scientific Conference on Power and Electrical Engineering of Riga Technical University (RTUCON), Riga, Latvia, 2021, pp. 1-6.

[2] M. Kasper, D. Bortis, and J. Kolar, "Classification and comparative evaluation of PV panel-integrated dc-dc converter concepts," *IEEE Trans. Power Electron.*, vol. 29, no. 5, pp. 2511–2526, May 2014.

[3] A. Chub, et al. "Analysis of Design Requirements and Optimization Possibilities of Partial Power Converter for Photovoltaic String Applications in DC Microgrids," *IEEE Access*, vol. 12, pp. 14605-14619, 2024.

[4] N. Yadav, N. Hassanpour, A. Chub, A. Blinov and D. Vinnikov, "Improved Maximum Power Point Tracking Algorithm for Step-Up/Down Partial Power Converters Operating Around Zero Partiality," *IEEE J. Emerg. Sel. Topics Power Electron.*, early access, doi: 10.1109/JESTPE.2024.3354843.

[5] J. Anzola et al., "Review of Architectures Based on Partial Power Processing for DC-DC Applications," *IEEE Access*, vol. 8, pp. 103405-103418, 2020.

[6] H. Chen, K. Sabi, H. Kim, T. Harada, R. Erickson, and D. Maksimovic, "A 98.7% efficient composite converter architecture with application tailored efficiency characteristic," *IEEE Trans. Power Electron.*, vol. 31, no. 1, pp. 101–110, Jan. 2016.

[7] D. Vinnikov, A. Chub, R. Kosenko, V. Sidorov and A. Lindvest, "Implementation of Global Maximum Power Point Tracking in Photovoltaic Microconverters: A Survey of Challenges and Opportunities," *IEEE J. Emerg. Sel. Topics Power Electron.*, vol. 11, no. 2, pp. 2259-2280, April 2023.

[8] V. Sidorov, A. Chub, D. Vinnikov and F. Z. Peng, "Survey of Topology Morphing Control Techniques for Performance Enhancement of Galvanically Isolated DC-DC Converters," *IEEE Open J. Ind. Electron. Soc.*, vol. 3, pp. 751-777, 2022.

[9] J. Zakis, D. Vinnikov and L. Bisenieks, "Some Design Considerations for Coupled Inductors for Integrated Buck-Boost Converters," *2011 International Conference on Power Engineering, Energy and Electrical Drives*, Malaga, Spain, 2011, pp. 1-6.

[10] R. Strzelecki and D. Vinnikov, "Models of the qZ-Converters", *Przeglad Elektrotechniczny*, vol. 86, no. 6, pp. 80-84, 2010.

[11] F. Flores-Bahamonde, H. Renaudineau, A. M. Llor, A. Chub and S. Kouro, "The DC Transformer Power Electronic Building Block: Powering Next-Generation Converter Design," *IEEE Ind. Electron. Mag.*, vol. 17, no. 1, pp. 21-35, March 2023.

[12] N. Hassanpour, A. Chub, A. Blinov and D. Vinnikov, "Soft-Switching Bidirectional Step-Up/Down Partial Power Converter With Reduced Components Stress," *IEEE Trans. Power Electron.*, vol. 38, no. 11, pp. 14166-14177, Nov. 2023.

[13] C. Liu, Z. Zhang, and M. A. E. Andersen, "Analysis and Evaluation of 99% Efficient Step-up/down Converter based on Partial Power Processing," *IEEE Trans. Ind. Electron.*, early access, doi: 10.1109/TIE.2022.3198241

[14] J. W. Zapata, S. Kouro, G. Carrasco, H. Renaudineau, and T. A. Meynard, "Analysis of partial power DC–DC converters for two-stage photovoltaic systems," *IEEE J. Emerg. Sel. Topics Power Electron.*, vol. 7, no. 1, pp. 591–603, Mar. 2019.

[15] N. Hassanpour, A. Chub, N. Yadav, A. Blinov and D. Vinnikov, "High-Efficiency Partial Power Converter for Integration of Second-Life Battery Energy Storage Systems in DC Microgrids," in IEEE Open Journal of the Industrial Electronics Society, doi: 10.1109/OJIES.2024.3389466.

[16] O. Abdel-Rahim, A. Chub, D. Vinnikov, and A. Blinov, ''DC integration of residential photovoltaic systems: A survey,'' *IEEE Access*, vol. 10, pp. 66974–66991, 2022.

[17] D. B. S. Alves, et al. "A single-stage three-port boost converter with high voltage gain based on the bidirectional version of the three-state switching cell," *2015 IEEE Applied Power Electronics Conference and Exposition (APEC)*, Charlotte, NC, USA, 2015, pp. 1934-1940.

[18] S. Kurm and V. Agarwal, "Hybrid energy storage system based on a novel reduced rating multi-input converter," *IEEE Trans. Power Electron.*, vol. 35, no. 11, pp. 12133–12142, Nov. 2020.

[19] O. Abdel-Rahim, A. Chub, A. Blinov, and D. Vinnikov, "Performance Evaluation of Step-Up/Down Current-Source Partial Power Converters for PV Applications," *RTUCON'2022*, Riga, Latvia, 2022, pp. 1-5.

[20] E. L. Carvalho, A. Blinov, A. Chub, I. Galkin and D. Vinnikov, "Multi-port i-AFE Converter for Grid-Interactive Buildings: Design Requirements and Efficiency Evaluation," 2023 IEEE 8th Southern Power Electronics Conference and 17th Brazilian Power Electronics Conference (SPEC/COBEP), Florianopolis, Brazil, 2023, pp. 1-5, doi: 10.1109/SPEC56436.2023.10408230.

[21] Y. Liu, Y. Hu, G. Chen and H. Wen, "Partial Power Processing Multi-port DC–DC Converter With Radial Module Connections," *IEEE Trans. Power Electron.*, vol. 37, no. 11, pp. 13398-13412, Nov. 2022.

[22] F. Hoffmann, et al. "A Multi-port Partial Power Processing Converter with Energy Storage Integration for EV Stationary Charging," *IEEE J. Emerg. Sel. Topics Power Electron.*, vol. 10, no. 6, pp. 7950-7962, Dec. 2022.

[23] R. Kosenko, A. Chub and A. Blinov, "Full-soft-switching high step-up bidirectional isolated current-fed push-pull DC-DC converter for battery energy storage applications," *IECON 2016 - 42nd Ann. Conf. of the IEEE Ind. Electron. Soc.*, Florence, Italy, 2016, pp. 6548-6553, doi: 10.1109/IECON.2016.7794014.